ADVANCED FUNCTIONAL MATERIALS
www.afm-journal.de

Control of the Electrical Properties in Spinel Oxides by Manipulating the Cation Disorder

Paul F. Ndione, Yezhou Shi, Vladan Stevanovic, Stephan Lany, Andriy Zakutayev, Philip A. Parilla, John D. Perkins, Joseph J. Berry, David S. Ginley, and Michael F. Toney**

In this work, the impact of cation disorder on the electrical properties of biaxially textured Co_2ZnO_4 and Co_2NiO_4 thin films grown by pulsed laser deposition are investigated using a combination of experiment and theory. Resonant elastic X-ray diffraction along with conductivity measurements both before and after post-deposition annealing show that Co_2ZnO_4 and Co_2NiO_4 exhibit opposite changes of the conductivity with cation disorder, which can be traced back to their different ground-state atomic structures, being normal and inverse spinel, respectively. Electronic structure calculations identify a self-doping mechanism as the origin of conductivity. A novel thermodynamic model describes the non-equilibrium cation disorder in terms of an effective temperature. This work offers a way of controlling the conductivity in spinels in a quantitative manner by controlling the cation disorder and a new design principle whereby non-equilibrium growth can be used to create beneficial disorder.

1. Introduction

Many complex oxides, including ceramics and minerals, have the potential to exhibit cation disorder over different crystallographic sites. In particular, ternary spinel oxides of the composition A_2BO_4,[1] are known to exhibit a large degree of cation disorder over the two types of lattice sites, those tetrahedrally (*Td*) or octahedrally (*Oh*) coordinated by the oxygen.[2,3] In a "normal" spinel, the B ions are found in the *Td* sites and the A ions in the *Oh* sites. In an "inverse" spinel, half of the A ions occupy the *Td* site and the other half occupy the *Oh* sites while the B ions occupy the remaining *Oh* sites. As a consequence, properties of spinels such as conductivity depend considerably on the level of disorder as the cations (often transition metals) can behave very differently depending whether they are octahedrally or tetrahedrally coordinated.[4,5] This makes spinel oxides ideal materials for studying structure-property relationships, and the understanding of the effects of the disorder could enable the controlled engineering of functionalities in device applications.

While often disorder results in decreased conductivity, theory has predicted that cation-site-occupancy disorder (hereinafter referred to as "cation disorder") should have a net hole producing effect for a special class of II-III *normal* spinels typified by Co_2ZnO_4 and denoted Doping Type 2.[6] Ni was predicted to be one of the best extrinsic dopants of Co_2ZnO_4 by Perkins et al.,[7] with Ni equilibrium solubility predicted to be only about 4%. Surprisingly, with increasing Ni content from Co_2ZnO_4 (0% Ni) to Co_2NiO_4 (100% Ni) electrical conductivity increased monotonically by more than four orders of magnitude. Co_2ZnO_4 a "normal" spinel and Co_2NiO_4, an "inverse" spinel that exhibits a large p-type conductivity[8] have raised considerable interest for potential applications in photovoltaics,[9,10] photodetectors,[11] oxygen reduction,[12] electrode catalysis,[13] and batteries.[14,15]

The objective of the present work is to establish the relationship between cation *Td*/*Oh* site disorder and conductivity in both Co_2ZnO_4 and Co_2NiO_4, to elucidate the electronic structure origin of the doping mechanism, and to develop a thermodynamic model that allows to describe, and ultimately control, the non-equilibrium disorder. In order to achieve this objective, we employ non-equilibrium films growth using pulsed laser deposition,[16] induce cation-site occupancy changes by post-deposition annealing,[3] and perform before and after annealing resonant elastic X-ray diffraction (REXD)[17,18] and conductivity measurements. In the theoretical part of this work, we use density functional calculations to determine the dependence of the electronic structure and of the formation enthalpy on the degree of disorder. In order to model non-equilibrium disorder, we combine experimental (site-occupancy measurements) and theoretical (enthalpy of disorder) information, and define an effective temperature,[19,20] i.e., the temperature at which a material in equilibrium would have the same degree of disorder as the film grown under non-equilibrium conditions. This concept provides a way to quantify the disorder due to non-equilibrium

Dr. P. F. Ndione, Dr. V. Stevanovic, Dr. S. Lany, Dr. A. Zakutayev, Dr. P. A. Parilla, Dr. J. D. Perkins, Dr. J. J. Berry, Dr. D. S. Ginley
National Renewable Energy Laboratory
Golden, Colorado, 80401, USA
E-mail: paul.ndione@nrel.gov
Y. Shi, Dr. M. F. Toney
SLAC National Accelerator Laboratory
Menlo Park, California, 94025, USA
E-mail: mftoney@slac.stanford.edu
Dr. V. Stevanovic
Colorado School of Mines
Department of Physics
Golden, Colorado, 80401, USA

DOI: 10.1002/adfm.201302535

growth techniques and offers the route for controlling the conductivity in spinels in a quantitative manner by controlling the cation disorder.

2. The Order Parameter Describing Inversion in Spinels

The stoichiometric spinel chemical formula can be written as $[A_{2-\lambda}B_{\lambda}](A_{\lambda}B_{1-\lambda})O_4$, with the two types of cations, A and B, occupying two types of interstitial sites in the slightly deformed fcc oxygen sublattice. Brackets denote octahedrally coordinated cation sites, whereas the tetrahedral sites are written in parentheses. The concentration of A cations on tetrahedral sites λ is referred to as the inversion parameter and takes values between 0 and 1. At low temperatures, spinels tend to order in either *normal* spinel structure (cubic Fd3m space group with $\lambda = 0$) in which all A cations occupy the octahedral and all B cation occupy the tetrahedral sites, or *inverse* spinel structure (tetragonal $P4_122$ with $\lambda = 1$) with half of A and all B cations distributed over the octahedral sites, while the tetrahedral sites ones are populated exclusively by the A cations (second half).

A deviation from these ground state configurations occurs with cation disorder – A and B cations exchange their sites. The disorder can be intrinsic (driven by entropy at increased temperatures) or due to non-equilibrium growth where the cations are more randomly distributed than in equilibrium. The point of maximal cation site randomness leads to an inversion parameter $\lambda = 2/3$ (see below). Thus, the inversion parameter can be expected to lie in the range $0 \leq \lambda \leq 2/3$ for "normal" spinels and in the range $2/3 \leq \lambda \leq 1$ for "inverse" spinels. It is also important to note, that while the degree of cation disorder grows with λ in normal spinels (e.g. Co_2ZnO_4), the trend is exactly the opposite, i.e. the cation disorder decreases with λ in spinels that are nominally inverse (e.g. Co_2NiO_4).

3. Cation Disorder Measurements and Electrical Properties

Polycrystalline samples of Co_2NiO_4 and Co_2ZnO_4 materials have previously been fabricated using sputtering.[10] However, the polycrystalline nature of the sputtered thin films on glass made it difficult to determine accurately the value of λ and as consequence, it was not possible to provide direct experimental evidence of site occupancy change in these materials after annealing. Hence, we fabricated biaxially textured spinel films on single crystal $SrTiO_3$ using PLD to ensure sufficiently high signal-to-noise ratio for REXD.

After deposition, the Co_2NiO_4 and Co_2ZnO_4 films are cut into half. The first half of the film is maintained in its as-deposited condition, while the second half of each sample is subjected to annealing in air at 650 °C (higher annealing temperature leads to phase segregation) for 1 h. We observe that annealing changes the conductivity of both materials. As reported in **Table 1**, for Co_2NiO_4, the conductivity increases from 33 ± 2 S/cm to 53 ± 3 S/cm after annealing, whereas for Co_2ZnO_4, the conductivity decreases from 10.5±0.8 S/cm to 3.2 ± 0.6 S/cm. All films exhibit positive Seebeck coefficients, confirming p-type conductivity for both Co_2NiO_4 and Co_2ZnO_4. Specifically, the measured Seebeck coefficients are 13.1 and 143.0 μV/K for as-deposited Co_2NiO_4 and Co_2ZnO_4, respectively, and 8 and 124.9 μV/K for annealed Co_2NiO_4 and Co_2ZnO_4, respectively, with an experimental uncertainty of ±0.8 μV/K for all measurements.

The REXD results for the as-deposited Co_2NiO_4 film are shown in **Figure 1**. We fit simulated energy-dependent REXD spectra to experimental diffraction intensities in order to determine site occupancies and degree of inversion. The open circles are integrated diffraction peak intensities corrected for absorption and the solid lines are the best fit calculated REXD spectra. The error bars to the integrated intensity are accumulated errors from correcting the filter attenuation and the beamline background, which is estimated as 1% of the integrated intensity in the raw data, by measuring the above-mentioned attenuation multiple times. The experimental data and simulation show a very good agreement, in both the "dip" at the absorption edges and in the regions that are a few hundred eV above or below the edges. Moreover, our simulation based on anomalous scattering factors captures the fine structures in the REXD (visible around 7800 eV in the Co edge data and around 8400 eV in the Ni edge data). The data analysis scheme is applied to all four samples studied here (see Supporting Information). Table 1 shows the summary of results related to the degree of inversion, chemical composition, electrical conductivities and site occupancies of all four samples. The results of the degree of inversion investigation in as deposited and annealed Co_2NiO_4 and Co_2ZnO_4 are presented in **Figure 2** (also shown in the Supporting Information). Three important points emerge from the analysis.

Table 1. Summary of fitted site occupancies and electrical properties of four samples. For Co_2NiO_4 (or Co_2ZnO_4), a higher Ni_{Oh} (or Zn_{Oh}) corresponds to a higher conductivity.

sample	composition	*Td* Site		*Oh* site		*Oh* site Degree of inversion	Conductivity [S/cm]
		Co	Ni/Zn	Co	Ni/Zn		
Co_2NiO_4 as-deposited	$Co_{2.01}Ni_{0.99}O_4$	0.88	0.12	0.57	0.43 ± 0.02	0.86 ± 0.04	33 ± 2
Co_2NiO_4 annealed	$Co_{1.99}Ni_{1.01}O_4$	0.98	0.02	0.52	0.48 ± 0.02	0.98 ± 0.04	53 ± 3
Co_2ZnO_4 as-deposited	$Co_{2.0}Zn_{1.0}O_4$	0.44	0.56	0.78	0.s22 ± 0.05	0.42 ± 0.09	10.5 ± 0.8
Co_2ZnO_4 annealed	$Co_{2.09}Zn_{0.91}O_4$	0.32	0.68	0.91	0.09 ± 0.045	0.2 ± 0.1	3.2 ± 0.6

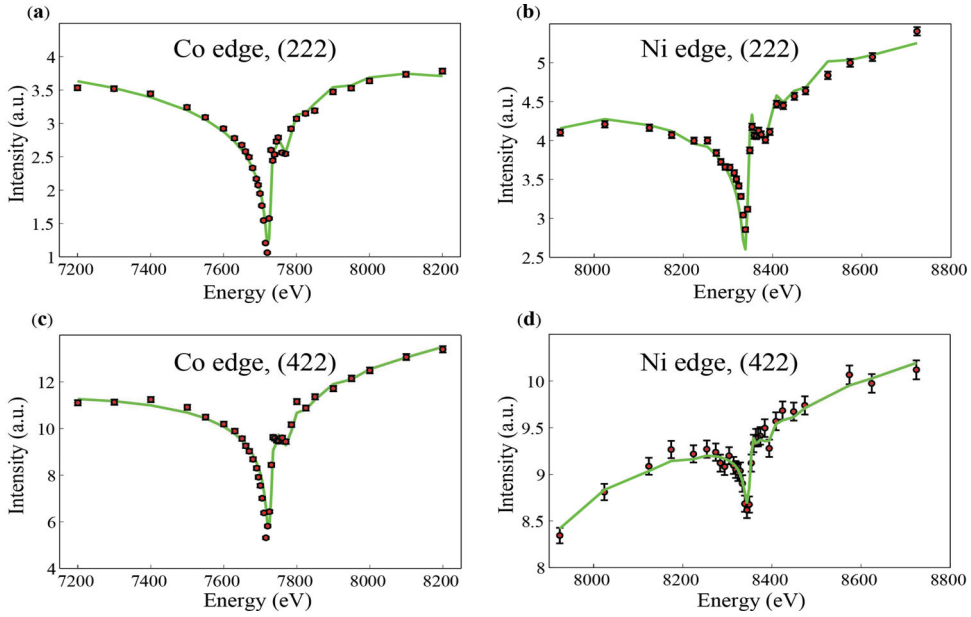

Figure 1. Fitted REXD results for the as-deposited Co_2NiO_4 sample. Open circles are experimental results corrected for absorption, whereas solid lines are calculated values based on the best fit. a) Data for (222) reflections near Co absorption edge, which indicates amount of Co occupying the *Oh* sites; b) data for (222) reflections near Ni absorption edge; c) (422) reflections near Co absorption edge, which indicates the amount of Co occupying the *Td* sites; d) (422) reflections near Ni absorption edge.

First, the biaxially textured Co_2ZnO_4 shows decreased Zn_{Oh} upon annealing (from to 22% to 9%). Co_2ZnO_4 is known as a normal spinel in its equilibrium state because Zn preferentially occupies the *Td* sites.[7] Annealing provides thermal energy necessary to overcome kinetic barriers, thereby driving the sample closer to thermodynamic equilibrium. For biaxially textured Co_2NiO_4, the annealed sample shows a slightly higher Ni_{Oh} (48%) than the as-deposited (43%) sample. Since

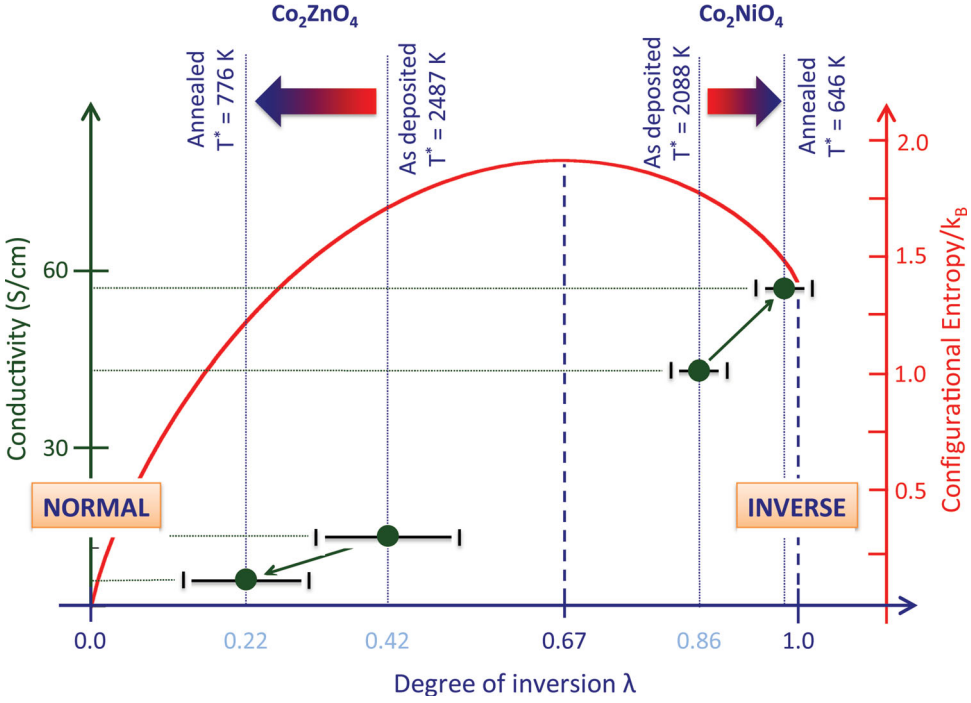

Figure 2. Opposite trends of the electrical conductivity as a function of the degree of inversion λ (green dots) in Co_2ZnO_4 and Co_2NiO_4 spinel oxides. Numerical values for the as-deposited and annealed films are provided in Table 1. Red curve shows the dependence of the configurational entropy on the degree of inversion as calculated from Equation (1). Arrows denote directions of the changes of λ parameter with annealing and T* are the effective temperatures quantifying the equilibrium conditions at which λ values equal those in the as grown and annealed samples (see text for details).

the Co_2NiO_4 spinel is more stable in its inverse configuration, we can attribute the change to the same thermodynamic driving force that changed the site occupancies in Co_2ZnO_4. Specifically, annealing decreases the degree of inversion in normal Co_2ZnO_4, whereas it increases the degree of inversion in Co_2NiO_4.

Second, the samples with higher Zn concentration on the *Oh* sites show a larger conductivity in Co_2ZnO_4, consistent with our previous experimental results[7] and with theoretical prediction that classifies Co_2ZnO_4 as a "doping-type 2" spinel;[6] namely, Co_2ZnO_4 is representative of a class of materials that can be self-doped p-type due to the unusual property that the cation disorder over the octahedrally and tetrahedrally coordinated lattice sites creates charge carriers. The classification of Co_2ZnO_4 as "doping-type 2" implies that Zn retains its +II oxidation states when replacing Co(III) on the octahedral site, thereby forming a hole-producing acceptor state. The Co_{Td} cation defects, in contrast, do not form an electrically active defect, since Co assumes a +II oxidation state on the tetrahedral site, thereby causing an isovalent substitution of Zn.[6,7] Thus, the conductivity reduction from as-deposited to annealed Co_2ZnO_4 is interpreted as resulting from the decreased Zn_{Oh} concentration, and the expected p-type (hole-carrier) conductivity is confirmed by positive Seebeck coefficients. The dependence of the conductivity on the Zn_{Oh} concentration (reduction of Zn_{Oh} from 0.22 to 0.09 and reduction of conductivity from 10.5 to 3.2 S/cm) is close to a direct proportionality. This finding could be explained by the prediction that Zn_{Oh} forms a shallow acceptor state,[7] implying that the hole carrier concentration increases proportionally with the Zn_{Oh} concentration.

Third, annealing Co_2NiO_4 increases Ni_{Oh} concentration, as expected from the fact that the ground state structure is an inverse spinel where all Ni cations are located on the *Oh* site. In contrast to the case of Co_2ZnO_4, the reduction of disorder due to annealing increases the conductivity in Co_2NiO_4. This observation suggests that Ni_{Oh} might act as hole producing in Co_2NiO_4 acceptor similar to Zn_{Oh} in Co_2ZnO_4. However, the dependence of the conductivity on the site occupancy is now rather far from a direct proportionality: Whereas the *Oh* site occupancy of Ni increases only moderately by 11% from 0.43 ± 0.02 to 0.48 ± 0.02, the conductivity increases by 60% from 33 ± 2 to 53 ± 3 S/cm (see Table 1). In this context, it is interesting to find that a previous investigation of site occupancy on Co_2NiO_4 samples using extended X-ray absorption fine structures (EXAFS) shows that the Ni on *Oh* sites has a mixed valence state of II and III.[21] Indeed, Ni(III) on *Oh* sites would produces no holes and not contribute to p-type conductivity. Our first principles calculations below show that Ni_{Oh} forms only a rather deep unoccupied gap state—which can be interpreted as Ni(III)—up to fairly large values of about $\lambda = 0.75$. Thus, up to the corresponding site Ni_{Oh} occupancy of $\lambda = 0.38$, one does not expect significant conductivity. However, at high degree of inversion approaching unity, the unoccupied gap states merge with the valence band forming a half-metallic state (see below). The conductivity is expected to increase strongly around this metal-insulator transition, explaining the observed non-proportionality between the Ni_{Oh} site occupancy and the conductivity.

4. Theoretical Description of Cation Disorder

4.1. Energetics

To understand and explain the opposite effect of the cation disorder on the conductivity of Co_2NiO_4 and Co_2ZnO_4 spinels, we performed a set of first principles, density functional theory (DFT) calculations for these two compounds at different atomic configurations, i.e. as a function of λ, the degree of inversion. We examine the dependence of the total energy (or enthalpy of formation) for Co_2ZnO_4 and Co on λ in the following way. For both compounds calculations are performed on normal ($\lambda = 0$), half inverse ($\lambda = 0.5$) and the tetragonal $P4_122$ ordered inverse ($\lambda = 1$) structures. The latter two structure types are constructed by performing one and two cation inversions (exchanging one octahedral A cation for one tetrahedral B cation) on the 14-atom primitive unit cell of the normal spinel structure, respectively. The tetragonal $P4_122$ ordered inverse has been shown by the point-ion electrostatics to be the likely ground state structure of inverse spinel oxides.[22] To model the effect of disorder we constructed a set of random structures using a 56-atom cubic supercell $Co_{16}(B)_8O_{32}$, with B = Zn or Ni. For Co_2ZnO_4 we choose three random configurations at each $\lambda = 0.5$ and $\lambda = 1$, whereas for the inverse Co_2NiO_4 we do the same only for $\lambda = 0.75$ and $\lambda = 1$. The reason is that for inverse spinels, structures with $\lambda < 0.67$ are not important as previously discussed and shown graphically in Figure 2. All calculations are performed within the GGA+U approach[23] and the projector augmented wave formalism[24] as implemented in the VASP code[25] Further details on the theoretical approach can be found in section 6.2.

In **Table 2** enthalpies of formation (ΔH_f) calculated using the fitted elemental-phase reference energies (FERE) approach[26]

Table 2. Calculated enthalpies of formation ΔH_f (in eV per formula unit) of Co_2NiO_4 and Co_2ZnO_4 for different atomic configurations corresponding to a given value of the degree of inversion λ and different supercell sizes (see text for details). Ground-state ΔH_f values are shown in bold. Last two columns list the α and β parameters of the O'Neil–Navrotsky modelf.[30] that are fitted to the calculated ΔH_f.

Compound		ΔH_f [eV/f.u.]				O'Neil–Navrotsky model	
		$\lambda = 0$	$\lambda = 0.5$	$\lambda = 0.75$	$\lambda = 1$	α [eV/f.u.]	β [eV/f.u.]
Co_2ZnO_4	14 atoms	**–10.59**	–9.93		–9.53	1.27	–0.18
Co_2ZnO_4	56 atoms		–10.00		–9.50		
Co_2NiO_4	14 atoms	–9.08	–9.16		**–9.27**	–0.15	–0.03
Co_2NiO_4	56 atoms			–9.21	–9.26		

for both Co_2ZnO_4 and Co_2NiO_4 in different atomic configurations are presented. To our knowledge, the ΔH_f values for these two compounds have not yet been reported. In case of 14-atom cell, ΔH_f of the normal ($\lambda = 0$), half inverse ($\lambda = 0.5$) and the ordered inverse (tetragonal $P4_122$ with $\lambda = 1$) are provided. In the case of the 56-atom unit cell, the ΔH_f are given averaged, at each λ, over the three random cation configurations described above. In agreement with the existing experimental data,[27,28] our calculated enthalpies of formation suggest that Co_2ZnO_4 adopts the normal spinel structure in the ground-state whereas Co_2NiO_4 is predicted to be inverse spinel.[27] These calculations also agree well with the sorting into normal and inverse spinels provided by the electrostatic model of Ref. [29]. The average ΔH_f values calculated on a 56-atom cell also support this result. Since in reality these systems are always disordered to a certain degree, the averaged ΔH_f can be used to fit the parameters α and β in the O'Neil–Navrotsky model,[30] expressing the inversion enthalpy $\Delta H_I = \alpha\lambda + \beta\lambda^2$ to quadratic order. The resulting values of α and β are also given in Table 2.

4.2. Free-Energy Model for Cation Disorder in Spinels

Free-energy minimization can in general be achieved by statistical sampling of all possible atomic configurations, taking into account their enthalpy differences. This approach was used in the Monte-Carlo simulations of Ref. [22], based on the electrostatic model of Ref. [29] for the enthalpies. If there exist no strong short-range order effects, one can approximately model the free energy using both enthalpies and entropies for random configurations. This approach is the basis of the O'Neil–Navrotsky model[30] which employs the above mentioned quadratic expansion of ΔH_I and the configurational entropy

$$\Delta S_C/k_B = -[\lambda \ln\lambda + (1-\lambda)\ln(1-\lambda) + \lambda\ln(\lambda/2) + (2-\lambda)\ln(1-\lambda/2)] \quad (1)$$

where k_B is the Boltzmann constant. The four terms in parentheses are nothing but the configurational entropies of two binary alloys, one on octahedral and the other on tetrahedral sublattice, with the degree of inversion λ defining their concentrations. As shown in Figure 2 by the $\Delta S_C/k_B$ dependence on λ (red curve), fully ordered normal spinel (e.g., Co_2ZnO_4 at low T) has zero configurational entropy, whereas the fully inverse spinel (e.g., Co_2NiO_4) has $\Delta S_C = 1.2\ k_B$ per formula unit corresponding to the entropy associated with random placement of the A and B atoms on the octahedral site.

Having a model for the energy (or enthalpy) of inversion and a model for the entropy of Equation (1) allows a simple estimate of the λ(T) dependence by constructing the Gibbs free energy

$$\Delta G = \alpha\lambda + \beta\lambda^2 - T(\Delta S_C + \Delta S_m) \quad (2)$$

with ΔS_m being the magnetic configurational entropy, and imposing the minimum condition at each temperature $\partial(\Delta G)/\partial\lambda = 0$. There is an additional contribution to entropy ΔS_m that can be approximated by the expression for the fully random arrangement of magnetic moments (just counting the number of configurations). For Co_2ZnO_4, local magnetic moments of octahedral Co^{3+} ions are zero and only tetrahedral Co which changes its oxidation state to 2+ carry magnetic moment as already shown in Ref. [7] leading to $\Delta S_m = k_B\lambda\ln 2$. This is also the case for Co ions in Co_2NiO_4, with the difference that in our calculations both octahedral and tetrahedral Ni ions have nonzero magnetic moments. Therefore $\Delta S_m(Co_2NiO_4) = k_B(1+\lambda)\ln 2$.

4.3. The Effect of Cation Disorder on the Electronic Structure

Returning to relationship between the cation disorder and the conductivity and carrier densities, we analyzed their electronic densities of states (DOS) and the dependence on atomic configuration. In **Figure 3** we show in black, for both Co_2ZnO_4 and Co_2NiO_4, spin resolved electronic densities of states (DOS) of the 14-atom unit cell normal ($\lambda = 0$), half inverse ($\lambda = 0.5$) and the ordered fully inverse ($P4_122$ with $\lambda = 1$) structures. The energy axes are referenced to the Fermi energy of the corresponding system. The DOS of both compounds in the normal spinel structure are similar. Co_2ZnO_4 system is nonmagnetic (octahedral Co^{3+} in the low spin configuration and tetrahedral Zn^{2+} is nonmagnetic) and has a band-gap of ~1.7 eV within the present DFT formalism, which generally tends to underestimate band gaps. Similarly, octahedral Co^{3+} is also in the low spin state in Co_2NiO_4, while the tetrahedral Ni^{2+} ions which carry magnetic moment of 2 μ_B are antiferromagnetically ordered. The calculated band gap is ~1.2 eV. After making one cation inversion in the 14-atom cell ($\lambda = 0.5$) both systems develop similar feature in their DOS. Namely, a defect-like empty state appears near the valence band maximum (VBM) which, as shown for Co_2ZnO_4,[7] is related to the acceptor-like Zn_{Oh} antisite defect which creates a hole in the valence band and leads to p-type conductivity, without being compensated by the corresponding Co_{Td} defect. This result explains the p-type conductivity of Co_2ZnO_4 at lower degrees of inversion below $\lambda = 0.5$. In Co_2NiO_4, however, the empty state inside the band gap lies at higher energies (see Figure 3), forming a deep level that does not support conductivity.

After two inversions in the 14-atom cell ($\lambda = 1.0$), the electronic structures of the systems become qualitatively different. The two tetrahedrally coordinated Co^{2+} ions in Co_2ZnO_4 order antiferromagnetically leading to the zero net magnetization and the defect-like level just above the VBM becomes a defect band separated by ~0.5 eV gap from the VBM. Thus, fully inverse Co_2ZnO_4 would be expected to be insulating. In Co_2NiO_4 the moments of tetrahedral Co are parallel as are those of Ni cations, but in the opposite direction. The defect like feature also broadens, but in the case of Co_2NiO_4 it merges with the valence band making the system half-metal. Thus, in Co_2NiO_4 there occurs a metal-insulator transitions at higher degrees of inversion between $\lambda = 0.5$ and $\lambda = 1$. These theoretical results also explain the observed opposite trends in electric conductivity. On the other hand, in Co_2ZnO_4, the conductivity decreases during annealing when the cation disorder is reduced towards the fully ordered $\lambda = 0$ normal spinel ground state which is nonconductive. In Co_2NiO_4, the conductivity is increased during annealing when cation disorder is reduced towards the $\lambda = 1$

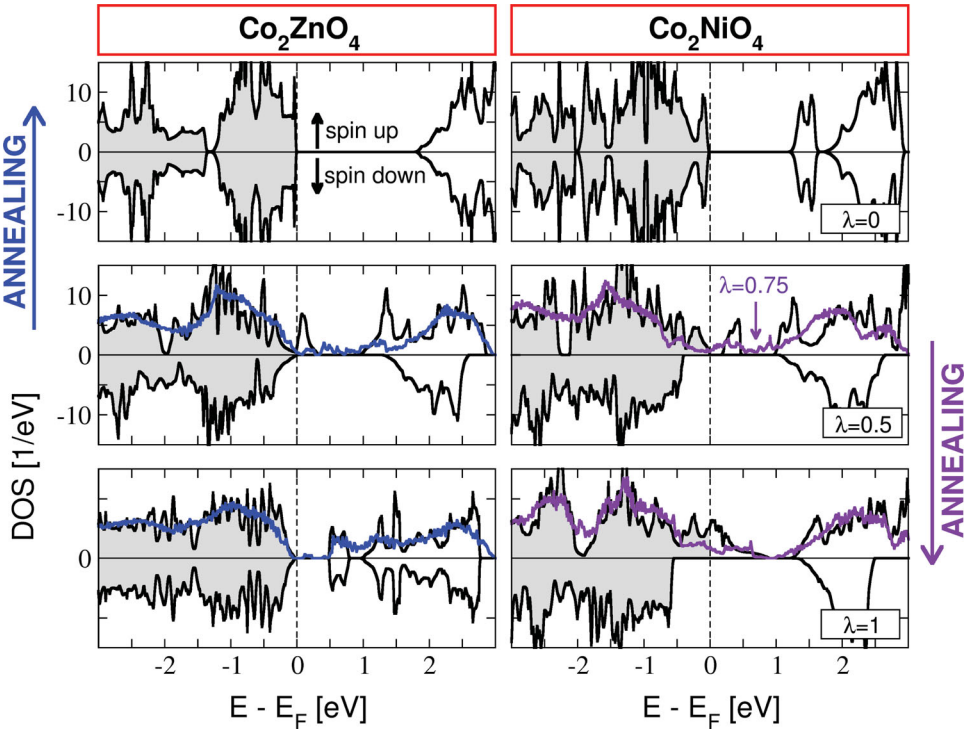

Figure 3. Calculated spin-resolved densities of states (black curves) for normal ($\lambda = 0$), half inverse ($\lambda = 0.5$) and $P4_122$ ordered inverse ($\lambda = 1$) spinel structure of Co_2ZnO_4 (left) and Co_2NiO_4 (right). The half inverse and ordered inverse structures are constructed by making one and two inversions on the normal spinel 14 atom primitive unit cell, respectively. Blue and indigo curves are the DOS averaged over the two spin channels and three random configurations with the same λ values, except the middle right box where the indigo curve represents the averaged DOS for $\lambda = 0.75$. Arrows denote the directions in which the structures transform in terms of the λ value due to annealing.

inverse spinel ground state which is conductive due to its half-metallic character.

While the 14-atom cell used to model the different degrees of inversion incorporate the cation exchange between *Oh* and *Td* sites, they do not fully account for the cation disorder on the *Oh* sublattice. We therefore considered additionally 56-atom cells with random realizations of disorder. The spin and structure averaged DOS are also shown in Figure 3, in blue for Co_2ZnO_4 and in indigo color for Co_2NiO_4 for which we plot the $\lambda = 0.75$ results instead of $\lambda = 0.5$ as these structures are closer to the real situation. In half inverted Co_2ZnO_4, the acceptor-defect feature close to the VBM becomes broader and extends to higher energies inside the gap, compared to the 14-atom model. However, at full inversion a deep state is formed similar as in the 14-atom model. These results corroborate the prediction that p-type conductivity in Co_2ZnO_4 should be reduced at high degrees of inversion, i.e., the maximum of the conductivity should occur below $\lambda = 0.5$. In Co_2NiO_4 the random structure with $\lambda = 0.75$ shows a broad impurity band with a minimum in the DOS at the Fermi level, indicating that the system is close to the metal-insulator transition mentioned above. For the fully inverse $\lambda = 1$ structure with disorder on the *Oh* sublattice, the DOS resembles to a large extent that of the ordered inverse spinel structure, specifically in regard of the half-metallic character. Thus, the randomized structures in the larger 56-atom cells confirm that the conductivity of Co_2NiO_4 should set in around $\lambda = 0.75$ and become maximal at full inversion.

These results show that the opposite trends in conductivities of Co_2NiO_4 and Co_2ZnO_4 with cation disorder, which are observed in experiments, are related to the difference of their atomic and electronic ground state structures. Indeed, the post-deposition annealing treatment brings Co_2ZnO_4 closer to an ordered and insulating ground-state normal spinel structure, whereas upon annealing Co_2NiO_4 changes its cation distribution toward an ordered, but in this case, more conductive ground-state inverse spinel structure. In addition the results provide an explanation on why Co_2NiO_4 is more conductive than Co_2ZnO_4.

4.4. Determination of an Effective Temperature Describing Non-Equilibrium Disorder

Using the O'Neil–Navrotsky model with the parameters α and β fitted from the first principles calculations, and the configurational and magnetic entropies ΔS_C and ΔS_m, Equation (2) describes the free energy as a function of temperature and the degree of inversion. Experimentally, the site occupancy measurements presented above provide the inversion parameter λ for both the as-grown (non-equilibrium) and annealed films. Assuming that annealing brings the films closer to an equilibrium state with respect to the cation disorder, one would expect that the measured inversion parameter minimizes the free energy ΔG (Equation (2) for the annealing temperature

T_a = 923 K. Evaluating the $\partial(\Delta G)/\partial\lambda = 0$ minimization condition from Equation (2) as a function of the temperature, we find that the measured λ = 0.22 and λ = 0.98 values correspond to the effective temperatures T^* = 776 K and T^* = 646 K in Co_2ZnO_4 and Co_2NiO_4, respectively. These temperatures lie slightly below the annealing temperature (923 K), which is plausible, because the samples are not instantaneously quenched to room temperature, so a certain amount of equilibration still takes place during the cool-down, until slow kinetics freeze-in the disorder at lower temperatures. Thus, the theoretical model based on first principles formation energies describes well the observed cation disorder in the annealed samples close to equilibrium.

Whereas equilibrium is a well-defined condition by means of the free energy minimization criterion, non-equilibrium conditions are generally more elusive. It is therefore important to define descriptors of non-equilibrium conditions such as those in the present thin-film growth. Thus, the present model and cation disorder measurements can be used to determine an effective temperature describing the non-equilibrium cation disorder in the as-grown samples (growth temperature: 623 K). Analyzing the measured inversion parameters λ = 0.42 and λ = 0.86 in the as-grown Co_2ZnO_4 and Co_2NiO_4 samples in the same way as above for the annealed samples yields the temperatures T^* = 2487 K and T^* = 2088 K, respectively. These effective temperatures describe the degree of disorder (inversion) at low-temperature non-equilibrium samples as being equivalent to the disorder under equilibrium conditions at the higher temperature T^*. It is important to note that T^* is only a descriptor of the disorder, and does not imply the equivalency to crystal growth at T^*. In fact, due to the temperature dependence of the chemical potentials which is not described by T^*, Co_2ZnO_4 decomposes into Co_3O_4 and ZnO around 1000 K, depending on the O_2 partial pressure.[31,32] The fact that growth of Co_2ZnO_4 above 1000 K is difficult in thermodynamic equilibrium, yet the as-grown samples have >2000 K effective temperatures, exemplifies how synthesis of materials far from equilibrium and practical use of their non-equilibrium properties can be achieved using physical vapor deposition techniques such as PLD or sputtering.

Once one understands (through electronic calculations) how disorder affects the observed properties (opposite effects in the conductivity) and has a model (effective temperature) that affords a handle to describe the non-equilibrium disorder in as-growth material, one comes into a position that allows to control the properties by manipulating the disorder. This paradigm shift away from the conventional situation where disorder is regarded as a complication or even nuisance defines the broad interest and high impact of our work, transcending by far the area of oxide spinels that served here as a test bed.

5. Conclusions

In this study, we have for the first time determined and quantified the relationship between the cation disorder and carrier concentration in spinels, using a unique combination of experimental and theoretical tools. Using first principles calculations for these two compounds at different atomic configurations, we found that in either material the p-type carrier density increases with the octahedral site-occupancy of the B atom (Zn or Ni), leading to a semiconducting behavior in the normal spinel Co_2ZnO_4, but to a half-metallic behavior in the inverse-spinel Co_2NiO_4. By using REXD and conductivity measurement on as-deposited and annealed p-type Co_2ZnO_4 and Co_2NiO_4 grown on $SrTiO_3$ by PLD, we have established the relationship between cation disorder and the the conductivity, thereby confirming the predicted site-occupancy and doping physics in A_2BO_4 spinels. Due to the different (normal vs. inverse spinel) equilibrium ground states, the annealing leads to opposite effects in the conductivity of Co_2ZnO_4 and Co_2NiO_4. This finding implies that the deliberate creation of non-equilibrium cation disorder during thin-film growth is an effective means to control the conductivity in these materials. We also determine an effective temperature as a descriptor for the cation disorder in as-grown films. The as-grown samples exhibit a disorder parameter corresponding to an effective temperature above 2000 K, much higher than the actual growth temperature of 350 °C (623 K). For annealed samples, the effective temperature in the range of 646–776 °C approaches the temperature of 650 °C (923 K) at which the samples are annealed. This concept provides a way to quantify the disorder that results from non-equilibrium growth, and to establish a link between theoretical thermodynamic models and thin film growth techniques.

6. Experimental Section

6.1. Material Fabrication and Characterizations

Materials and Fabrication: Co_2NiO_4 or Co_2ZnO_4 spinel oxide thin films were grown on (100) $SrTiO_3$ substrates by pulsed laser deposition using a stainless steel high vacuum deposition chamber and a KrF excimer laser (Spectra-Physics operating at 248 nm with a pulse duration of 25 ns). The laser was operated at 10 Hz and the beam was focused through a 40 cm lens onto a commercial 1 inch Co_2NiO_4 or Co_2ZnO_4 rotating target (purity 99.99%) at a 45° angle, with a laser fluence of 2 J/cm^2 on the target surface. The target-substrate distance was fixed at 5 cm. Prior to the depositions, the growth chamber was evacuated to a base pressure of 10^{-7} Torr using a turbomolecular pump. The depositions were performed at a substrate temperature of 350 °C under 2 mTorr of oxygen pressure. Subsequent to the depositions, the Co_2NiO_4 and Co_2ZnO_4 films were cut into half. Half of each sample was subjected to annealing in air at 650 °C for 1 h then cooled down to room temperature whereas the other half remained un-annealed.

Structural and Chemical Characterizations: The films orientation and thickness of 130 nm were determined by X-ray diffraction, using a Cu $K\alpha$ radiation (Rigaku Ultima IV) and spectroscopic ellipsometry (J. A. Woollam M-2000S) respectively. X-ray fluorescence (XRF) measurements to determine the composition of the films were performed on a Matrix Metrologies MaXXi 5 with W anode, 800-µm collimator and 300s scan time. The resulting spectra were modeled using the MTF-FP software to obtain the chemical composition of the samples.

Electrical Characterizations: The measurement of the electrical conductivity was carried out by using the four-point probe method. The current was applied by a Keithley 6221 DC and AC current source and the voltage measured with a Keithley 2182 voltmeter. To determine the conductivity type of the samples, Seebeck coefficient measurements were performed on a custom-built transport measurement instrument described previously[33] and designed to measure the resistivity, Hall mobility, Seebeck coefficient, and Nernst coefficient.

Cation Disorder Determination: The REXD measurements were performed on the six-circle diffractometer beamline 7–2 of the Stanford Synchrotron Radiation Lightsource (SSRL) at the SLAC National Accelerator Laboratory. The incident X-ray energy was varied with a double crystal Si(111) monochromator. A Vortex detector was employed to measure X-ray intensity. Phi scans for (222) and (422) reflections were performed at various energies near the absorption K edges of Co, Ni, and Zn. Filters were inserted in front of the detector to protect it from the strong X-rays diffracted from the textured films. The filter attenuation was recorded in a direct beam configuration and these were used to correct the data before we fit the site occupancies. The fluorescence X-ray absorption spectrum (XAS) was obtained in order to experimentally extract the imaginary term f_2 of the structure factor, measured over the same energy range in which REXD data were acquired (see Supporting Information).

6.2. Theory

In this work we use the GGA+U approach of Ref. [23] employing the generalized gradient approximation (GGA) to density functional theory in the PBE functional form[34] with the additional Hubbard like term describing the onsite Coulomb interaction (U). This is required to overcome the limitations of the GGA alone and account, in an approximate way, for the electronic correlations present in compounds containing transition metals (oxides in particular). Concerning the choice of U, which is an external parameter in this approach, we follow Ref. [26] and use fixed U = 3 eV value for both Co and Ni (U = 0 eV for other atom types). It is shown in Ref. [26] that this is a good choice for calculating accurate compound enthalpies of formation. In all calculations spin degrees of freedom have been taken into account explicitly. In case of 14-atom structures, the results correspond to the lowest energy magnetic configuration obtained by initializing all possible combinations of magnetic moments on the 14-atom unit cell and letting the system relax. In the case of random structures with 56 atoms, for each random atomic configuration, magnetic moments are initialized in 10 different ways (ferromagnetic plus 9 random magnetic configurations) and all results are averaged over different atomic and magnetic configurations and both spin directions, but only structures with total energies in 0.170 eV (temperature of ~2000 K) window above the lowest energy for a given λ are considered. This is an approximate way to account both for the atomic as well as the magnetic disorder present in these systems. Further details of our computational approach have been described previously.[26]

Supporting Information

Supporting Information is available from the Wiley Online Library or from the author.

Acknowledgements

P. F. Ndione, Y. Shi, and V. Stevanovic contributed equally to this work. This material is based upon work supported as part of the "Center for Inverse Design", an Energy Frontier Research Center funded by the US Department of Energy, Office of Science, Office of Basic Energy Sciences under Award Number DE-AC36–08GO28308 to NREL. Portions of this research were carried out at the Stanford Synchrotron Radiation Lightsource (SSRL), a Directorate of SLAC National Accelerator Laboratory and an Office of Science User Facility operated for the US Department of Energy Office of Science by Stanford University. We acknowledge helpful discussions with Dr. Tula R. Paudel with regard to the Doping Type theory. We also thank Ronald Marks, Charles Troxel, Jr., and Bart Johnson for their assistance at the SSRL facilities. V.S. acknowledges administrative support of REMRSEC at Colorado School of Mines. The spacing of Equation 1 was corrected on February 5, 2014.

Received: July 28, 2013
Revised: September 12, 2013
Published online: October 29, 2013

[1] While a commonly used formula for III-II spinel is AB_2O_4, we adopt the notation A_2BO_4 to remain consistent with previous work we have reported on A_2BX_4 compounds.
[2] P. Barpanda, S. K. Behera, P. K. Gupta, S. K. Pratihar, S. Bhattacharya, *J. Eur. Ceram. Soc.* **2006**, *26*, 2603.
[3] B. J. Wood, R. J. Kirkpatrick, B. Montez, *Am. Mineralogist* **1986**, *71*, 999.
[4] M. Dekkers, G. Rijnders, D. H. A. Blank, *Appl. Phys. Lett.* **2007**, *90*, 021903.
[5] E. J. W. Verwey, F. de Boer, J. H. van Santen, *J. Chem. Phys.* **1948**, *16*, 1091.
[6] T. R. Paudel, A. Zakutayev, S. Lany, M. d'Avezac, A. Zunger, *Adv. Funct. Mater.* **2011**, *21*, 4493.
[7] J. Perkins, T. Paudel, A. Zakutayev, P. Ndione, P. Parilla, D. Young, S. Lany, D. Ginley, A. Zunger, N. Perry, Y. Tang, M. Grayson, T. Mason, J. Bettinger, Y. Shi, M. Toney, *Phys. Rev. B* **2011**, 84.
[8] R. Owings, G. Exarhos, C. Windisch, P. Holloway, J. Wen, *Thin Solid Films* **2005**, *483*, 175.
[9] P. F. Ndione, A. Garcia, N. E. Widjonarko, A. K. Sigdel, K. X. Steirer, D. C. Olson, P. A. Parilla, D. S. Ginley, N. R. Armstrong, R. E. Richards, E. L. Ratcliff, J. J. Berry, *Adv. Energy Mater.* **2013**, *3*, 8.
[10] A. Zakutayev, T. R. Paudel, P. F. Ndione, J. D. Perkins, S. Lany, A. Zunger, D. S. Ginley, *Phys. Rev. B* **2012**, *85*, 085204.
[11] L. Hu, L. Wu, M. Liao, X. Fang, *Adv. Mater.* **2011**, *23*, 1988.
[12] A. C. D. Angelo, E. R. Gonzalez, L. A. Avaca, *Int. J. Hydrogen Energy* **1991**, *16*, 1.
[13] B. Cui, H. Lin, J. B. Li, X. Li, J. Yang, J. Tao, *Adv. Funct. Mater.* **2008**, *18*, 1440.
[14] R. Alcantara, M. Jaraba, P. Lavela, J. L. Tirado, *Chem. Mater.* **2002**, *14*, 2847.
[15] B. Liu, J. Zhang, X. Wang, G. Chen, D. Chen, C. Zhou, G. Shen, *Nano Lett.* **2012**, *12*, 3005.
[16] D. B. Chrisey, G. K. Hubler, *Pulsed Laser Deposition of Thin Films* Wiley-VCH, **2003**.
[17] G. Materlik, C. J. Sparks, K. Fischer in *Theory and Applications* North-Holland, Amsterdam, **1994**.
[18] Y. Joly, S. D. Matteo, O. Bunau, *Eur. Phys. J.—Special Topics* **2012**, *208*, 21.
[19] S. D. Baranovskii, B. Cleve, R. Hess, P. Thomas, *J. Non-Cryst. Solids* **1993**, *166*, 437.
[20] I. Fernández-Martínez, J. L. Costa-Krämer, F. Briones, *J. Appl. Phys.* **2008**, 103.
[21] J. F. Marco, J. R. Gancedo, M. Gracia, J. L. Gautier, E. Rios, F. J. Berry, *J. Solid State Chem.* **2000**, *153*, 74.
[22] V. Stevanovic, M. d'Avezac, A. Zunger, *J. Am. Chem. Soc.* **2011**, *133*, 11649.
[23] S. L. Dudarev, G. A. Botton, S. Y. Savrasov, C. J. Humphreys, A. P. Sutton, *Phys. Rev. B* **1998**, *57*, 1505.
[24] P. E. Blöchl, *Phys. Rev. B* **1994**, *50*, 17953.
[25] G. Kresse, J. Furthmuller, *Comput. Mater. Sci.* **1996**, *6*, 15.
[26] V. Stevanovic, S. Lany, X. Zhang, A. Zunger, *Phys. Rev. B* **2012**, *85*, 115104.
[27] O. Knop, K. I. G. Reid, Sutarno, Y. Nakagawa, *Canadian J. Chem.* **1968**, *46*, 13.
[28] K. Krezhov, P. Konstantinov, *J. Phys. Condens. Matter* **1993**, *5*, 9287.

[29] V. Stevanovic, M. d'Avezac, A. Zunger, *Phys. Rev. Lett.* **2010**, 105.
[30] H. S. C. O'Neill, A. Navrotsky, *Am. Mineralogist* **1983**, *68*, 181.
[31] N. H. Perry, T. O. Mason, C. Ma, A. Navrotsky, Y. Shi, J. S. Bettinger, M. F. Toney, T. R. Paudel, S. Lany, A. Zunger, *J. Solid State Chem.* **2012**, *190*, 143.
[32] T. R. Paudel, S. Lany, M. d'Avezac, A. Zunger, N. H. Perry, A. R. Nagaraja, T. O. Mason, J. S. Bettinger, Y. Shi, M. F. Toney, *Phys. Rev. B* **2011**, 84.
[33] D. L. Young, T. J. Coutts, V. I. Kaydanov, *Rev. Sci. Instrum.* **2000**, *71*, 462.
[34] J. P. Perdew, K. Burke, M. Ernzerhof, *Phys. Rev. Lett.* **1996**, *77*, 3865.